Chen et al. Nanoscale Research Letters (2016) 11:295
DOI 10.1186/s11671-016-1493-7

Nanoscale Research Letters

NANO EXPRESS Open Access

CdS/CdSe Co-sensitized Solar Cells Based on Hierarchically Structured SnO_2/TiO_2 Hybrid Films

Zeng Chen, Chaochao Wei, Shengjun Li*, Chunli Diao, Wei Li, Wenping Kong, Zhenlong Zhang and Weifeng Zhang*

Abstract

SnO_2 nanosheet-structured films were prepared on a fluorine-doped tin oxide (FTO) substrate using ZnO nanosheet as template. The as-prepared SnO_2 nanosheets contained plenty of nano-voids and were generally vertical to the substrate. TiO_2 nanoparticles were homogeneously deposited into the intervals between the SnO_2 nanosheets to prepare a hierarchically structured SnO_2/TiO_2 hybrid film. The hybrid films were co-sensitized with CdS and CdSe quantum dots. The sensitized solar cells assembled with the SnO_2/TiO_2 hybrid film showed much higher photoelectricity conversion efficiency than the cells assembled with pure TiO_2 films. The lifetime of photoinduced electron was also investigated through electrochemical impedance spectroscopy, which showed that the SnO_2/TiO_2 hybrid film electrode is as long as the TiO_2 film electrode.

Keywords: SnO_2 nanosheet, SnO_2/TiO_2 hybrid films, Quantum dots, CdS, CdSe

Background

In recent years, quantum dot (QD)-sensitized solar cells have attracted remarkable attention because of the multiple exciton generation characters. The theoretical energy conversion efficiency of QD-sensitized solar cells (QDSCs) was calculated to be about 44.4 % which is much higher than that of the organic dye-sensitized solar cells [1]. Many narrow bandgap semiconductor QDs, such as PbS, CdS, and CdSe, have been extensively used to sensitize TiO_2 photoanode [2–5]. Compared with TiO_2, SnO_2 has many advantages. Firstly, the energy gap of SnO_2 is about 3.6 eV which may reduce the effect of UV light in the sunlight on the solar cell performance and improve their long-term stability [6]. Secondly, the electron mobility of SnO_2 is about 150 $cm^2\ V^{-1}\ s^{-1}$ which is much higher than that of TiO_2 (1 $cm^2\ V^{-1}\ s^{-1}$) [7, 8]. Thirdly, SnO_2 films which are suitable for sensitized solar cells could be obtained without high temperature calcination [9, 10]. Therefore, some teams began to apply nanoporous SnO_2 as photoanodes in QD-sensitized solar cells. Hossain et al. found that $TiCl_4$ treatment can significantly increase the open circuit photovoltage of CdSe QD-sensitized SnO_2 solar cells [11]. Then, they co-sensitized SnO_2 films with CdS and CdSe QDs and obtained much higher short circuit current (J_{SC}, 17.40 mA cm^{-2}) than that of TiO_2 film based QD-sensitized solar cells [12]. Cánovas et al. studied the electron transfer processes from PbSe quantum dots to SnO_2 and found that the injection time of the photoexcited electron was vitally affected by the QD size [13]. Xiao et al. found that the shape of SnO_2 might affect the photovoltage of SnO_2-based QDSCs. They applied highly ordered SnO_2 inverse opal films to QDSCs and obtained high open circuit voltage (V_{OC}, 700 mV) and high short circuit current (10.13 mA cm^{-2}). The total photoelectric transfer efficiency was about 4.37 % [14].

Specific nanostructure of nanoparticles, such as nanorod, nanosheet, and nanowire, could bring some distinctive properties. Some teams had attempted to prepare SnO_2 nanosheets. Li Y et al. synthesized SnO_2 nanosheets by hydrothermal method from $SnCl_2$ and NaOH in ethanol/water solution [15]. Fei L et al. prepared SnO_2 nanosheets using graphite sheets as template [16]. Dong

* Correspondence: Lishengjun1011@126.com; wfzhang@henu.edu.cn
Key Laboratory of Photovoltaic Materials of Henan Province and School of Physics and Electronics, Henan University, Kaifeng 475001, People's Republic of China

CJ et al. obtained Pt-functionalized SnO_2 nanosheets by a facial solution combustion method [17].

In this experiment, we prepared SnO_2 nanosheet-structured films using ZnO nanosheet as template. The as-prepared SnO_2 nanosheets contain plenty of nanovoids and are generally vertical to the substrate, which should provide an efficient collection path for the photoinduced electron. To obtain SnO_2/TiO_2 composite films, TiO_2 nanoparticles were deposited on SnO_2 nanosheet through electrophoresis method. And these films were introduced into QDSCs. From the band energy structure of SnO_2 and TiO_2, we can see that the electron can transfer from the conduction band of TiO_2 to that of SnO_2 shown in Fig. 1a. So the SnO_2/TiO_2 composite films could combine the advantages of both SnO_2 nanosheet and TiO_2 particle. The photoexcited charges were separated efficiently on the surface of TiO_2 nanoparticles. Thereafter, photoinduced electron will be collected by SnO_2 nanosheets and transported to the fluorine-doped tin oxide (FTO) substrate fluently. The schematic diagram of these processes is shown in Fig. 1b.

Methods

Materials

Zinc nitrate hexahydrate ($Zn(NO_3)_2{\cdot}6H_2O$), zinc acetate ($Zn(CH_2COO)_2$), ammonium hexafluorostannate ($(NH_4)_2SnF_6$), boric acid (H_3BO_3), cadmium acetate ($Cd(CH_2COO)_2$), selenium powder (Se), sodium thiosulfate ($Na_2S_2O_3.5H_2O$), nitrilotriacetic acid trisodium salt ($C_6H_8NNa_3O_7$), copper nitrate trihydrate ($Cu(NO_3)_2{\cdot}3H_2O$), and sodium sulfide (Na_2S) were all purchased from Sinopharm Chemical Reagent Co. (SCRC, China). Ethanol and methanol were purchased from Aladdin Reagent Co. (China) with a purity >99.9 %. All of these materials were used as received without any further purification.

The electrodeposition of ZnO nanosheets was carried out in a simple three-electrode glass cell. The precursor solution (for ZnO deposition) consisted of 0.05 M $Zn(NO_3)_2{\cdot}6H_2O$ and 0.1 M KCl. The working electrode was FTO glass substrates (10 × 10 mm). The reference electrode was Ag/AgCl electrode with saturation potassium chloride aqueous solution, and the counter electrode was Pt metal sheet. The distance between the working electrode and the counter electrode was about 3.5 cm. The deposition temperature was fixed at 70 °C by an oil bath. The deposition potential was controlled to be −1.1 V. The deposition time was controlled to be 30 min unless specially instructed. The deposited samples were cleaned with deionized water, dried at room temperature, and annealed at 450 °C for 30 min in the air atmosphere. The deposition time was controlled to be 30 min. For the formation of SnO_2 layer, the ZnO nanosheets were then immersed in a mixture of 3 mL 0.15 mol L^{-1} $(NH_4)_2SnF_6$, 1 mL 0.5 mol L^{-1} H_3BO_3, and 1 mL deionized water [18]. The immersion time was 4 h to convert all ZnO nanosheets to SnO_2 nanosheets. The SnO_2 nanosheets were cleaned with deionized water, dried at room temperature, and sintered at 500 °C for 30 min under air atmosphere. Then, the SnO_2 nanosheet-structured films were immersed into 40 mM $TiCl_4$ aqueous solution at 70 °C. The immersion time was controlled to be 40 min. The $TiCl_4$-treated SnO_2 films were annealed at 500 °C for 30 min under air atmosphere. Then, commercial TiO_2 nanoparticles (P25) were deposited on the SnO_2 nanosheet through electrophoresis method in a colloid solution (0.5 g P25 dispersed in a mixture of 8 mL butanol, 4 mL isopropanol, and 2 mL ethanol). In the electrophoresis processes, an FTO glass (1 × 2 cm^2, 15 Ω sq^{-1}; OPV Tech) was used as the cathode and another FTO glass was used as the anode. The distance between the two electrodes was maintained at 1 cm, and the DC power supply was set at 48 V. The electrophoresis

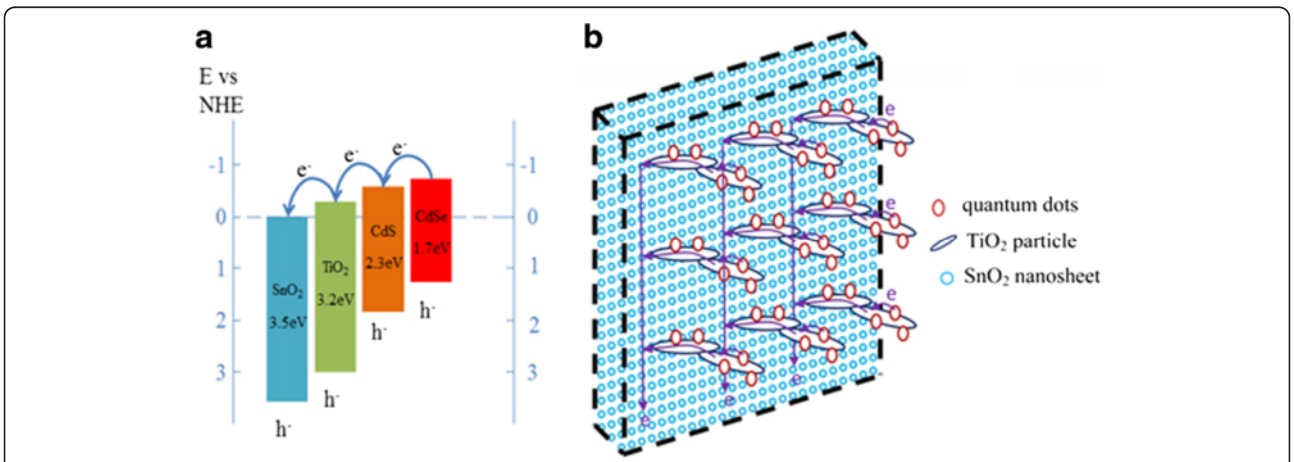

Fig. 1 Diagrammatic sketch of band energy **(a)** and structure **(b)** of SnO_2/TiO_2 hybrid film

time is 10 s. The SnO_2/TiO_2 hybrid films were sintered at 500 °C for 30 min.

CdS/CdSe Co-sensitized Photoanodes and Solar Cell Device Fabrication

CdS and CdSe quantum dots were deposited on these nanoporous films (pure SnO_2 film, $TiCl_4$-treated SnO_2 film, SnO_2/TiO_2 hybrid film, or pure TiO_2 film) in sequence. The deposition process was summarized as follows. Firstly, the nanoporous films were sensitized with CdS quantum dots by successive ionic layer adsorption and reaction (SILAR) method. The deposition process was summarized as follows: (i) The pure ZnO and ZnO/TiO_2 composite samples were firstly dipped in the 0.1 M $Cd(NO_3)_2$ ethanol solution for 1 min, then rinsed with ethanol for 1 min, followed by dipping in the 0.1 M methanol solution for 1 min and then rinsing with methanol for 1 min. (ii) The former processes were repeated 14 times in order to grow sufficient amount of CdS QDs on the films. Secondly, the CdS-sensitized films were immersed in a mixture of aqueous solution, 0.2 mol L^{-1} Na_2SeSO_3, 0.16 mol L^{-1} $C_6H_8NNa_3O_7$(NTA-3Na), and 0.08 mol L^{-1} $Cd(CH_2COO)_2$ (V:V:V = 1:1:1), for 4 h. Thirdly, the CdS/CdSe co-sensitized films were passivated with ZnS by immersion into 0.1 mol L^{-1} $Zn(CH_2COO)_2$ and 0.1 mol L^{-1} Na_2S aqueous solution in sequence. For QDSCs fabrication, CuS counter electrodes were prepared according to the reported literature [19]. The polysulfide aqueous solution of 1 mol L^{-1} Na_2S, 1 mol L^{-1} S, and 0.1 mol L^{-1} NaOH was used as the QDSCs electrolyte.

Measurement and Characterization

The crystalline phase of the samples was characterized by DX-2700 X-ray diffractometer (XRD) with a monochromatized CuK irradiation ($k = 0.154145$ nm). The morphology was studied using JSM-7001F field emission scanning electron microscope (FE-SEM). Energy dispersive spectroscopy analysis (EDS) was obtained from Bruker-ASX (Model Quan-Tax 200).

The assembled QDSCs were tested under simulated sunlight (AM 1.5G illumination) from a Newport Oriel Solar Simulator (model 94043A, Oriel) using Keithley 2440 Source Meter. The light intensity was calibrated with a standard Si solar cell provided by Newport Oriel. The active cell area of the testing QDSCs was 0.25 cm^2. The monochromatic incident photon-to-electron conversion efficiency (IPCE) was measured using an IPCE system (QS 500ADX, Crowntech, Inc.). The testing ranged from 300 to 800 nm. A 150-W tungsten halogen lamp was used as the light source to generate a monochromatic beam. A silicon solar cell was used as the reference during the IPCE measurement. An electrochemistry workstation (IM6) was used to investigate the electrochemical impedance spectra (EIS) of QDSCs. This measurement was also carried out with the same structured QDSCs as that used in the former experiments. The impedance measurement of QDSCs was recorded under dark condition at the bias potential of −0.6 V over a frequency range of 0.1–1 MHz with an AC amplitude of 10 mV.

Results and Discussion

ZnO nanosheet-structured film was firstly electrodeposited on FTO substrate. Then, the ZnO nanosheet-structured film was immersed in $(NH_4)_2SnF_6$ aqueous solution. The SnF_6^{2-} ions in the solution will hydrolyze and form SnO_2 nanoparticles on the surface of ZnO nanosheets following Eq. 1. The generated F^- ion in Eq. 1 could be trapped by boric acid as described in Eq. 2. The H^+ in HBF_4 would dissolve ZnO into the solution. If the immersion time was long enough, all the ZnO nanosheets on the FTO substrate might be totally dissolved into the solution. As a result, pure SnO_2 nanoporous nanosheet film was prepared. The chemical reactions in the treatment process might proceed with the following mechanisms [18]:

$$SnF_6^{2-} + 2H_2O \rightarrow SnO_2 + 6F^- + 4H^+ \quad (1)$$

$$H_3BO_3 + 4HF \rightarrow HBF_4 + 3H_2O \quad (2)$$

$$ZnO + 2H^+ \rightarrow Zn^{2+} + H_2O. \quad (3)$$

Figure 2 shows the XRD patterns for the pure ZnO films before and after 4 h immersion in the $(NH_4)_2SnF_6$ aqueous solution. Before the treatment of $(NH_4)_2SnF_6$ aqueous solution, there is a series of narrow peaks at 31.76°, 34.4°, 36.24°, 47.56°, and 56.6° in the X-ray diffraction spectra. These peaks indicate the growth of wurtzite-structured ZnO (hexagonal phase, space group

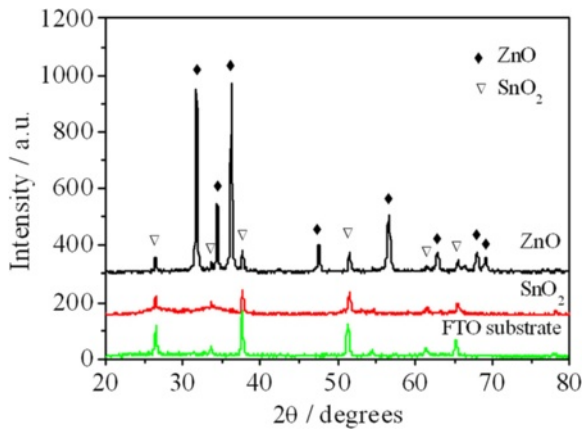

Fig. 2 XRD of FTO substrate and the prepared pure ZnO and SnO_2 films

P63mc) (JCPDS database card no. 36-1451). Other peaks are all in accordance with the diffraction peaks of the FTO substrate. After 4 h of immersion in the $(NH_4)_2SnF_6$ aqueous solution, no diffraction peaks of ZnO can be found in the spectrum which indicates that all ZnO nanosheets have been dissolved into the solution. The ultimate sample consists of pure SnO_2.

Figure 3a–c shows the top view and cross section of the prepared pure SnO_2 nanosheet film. The as-prepared SnO_2 films are not as regular as ZnO films, but it maintains the nanosheet structure. And the SnO_2 sheets are also generally vertical to the substrate. The microstructure of the SnO_2 nanosheet is much different from that of ZnO. There are plenty of homogeneous nano-voids distributed between SnO_2 nanoparticles. These nano-voids are suitable for the deposition of TiO_2 nanoparticles and quantum dots. The thickness of the film is about 6 μm.

The conduction band edge of SnO_2 is 0.4 V (versus the standard hydrogen electrode (SHE)) which is more positive than that of TiO_2. Photoexcited electrons in the conduction band of SnO_2 undergo serious back reactions [20]. Coating SnO_2 with thin layers of TiO_2 is an efficient way to inhibit these back reactions. So the as-prepared SnO_2 sheet films were treated in 40 mM $TiCl_4$ aqueous solution at 70 °C for 40 min for the covering of a passivation layer of TiO_2. Then, commercial TiO_2 nanoparticles (P25) were deposited on the SnO_2 sheets through electrophoretic method. Figure 3d shows the cross section of the TiO_2 nanoparticle-covered SnO_2 film. It can be seen that TiO_2 nanoparticles were homogeneously filled in the intervals between SnO_2 nanosheets. From the cross section of SnO_2/TiO_2 hybrid film, the SnO_2 nanosheets become so distinct that we can almost not found them. This change of SnO_2 might be caused by the mild dissolution of SnO_2 in $TiCl_4$ treatment. And the TiO_2 nanoparticles were efficiently coated on SnO_2 skeleton.

X-ray EDS was carried out to confirm the final composition of the SnO_2/TiO_2 hybrid film. The EDS spectra are shown in Fig. 4. The peaks at about 3.4, 3.6, 4.44, and 4.82 KeV should correspond to Sn(La), Sn(Lb), Ti(Ka), and Ti(Kb), respectively. The composition analysis revealed that the ratio between Sn and Ti was about 13.5:86.5. The element distribution diagrams are also given in Fig. 4b–d. It can be seen that Sn element exists throughout the whole films. At the bottom of the film, there is a gathering of Sn element which should be attributed to the F-coated SnO_2 layer on the glass substrate. The Ti element was homogeneously filled in the SnO_2 frameworks.

To investigate the effects of $TiCl_4$ treatment and coverage of TiO_2 nanoparticles on the photovoltaic characteristics of the SnO_2 films, these nanoporous films (pure SnO_2 film, $TiCl_4$-treated SnO_2 film, SnO_2/TiO_2 hybrid film, or pure TiO_2 nanoparticle film) were all co-sensitized with CdS and CdSe quantum dots. They were assembled with CuS counter electrodes, separately, to form a complete QDSC. The *J-V* curves of the former assembled QDSCs are shown in Fig. 5. The pure SnO_2 nanosheets film shows poor photovoltaic characteristics. After $TiCl_4$ treatment, the J_{SC} and V_{OC} increased from 2.9 mA cm^{-2} and 25 mV to 7.7 mA cm^{-2} and 161 mV, respectively. These characteristic parameters are significantly improved because the recombination reaction at the surface of SnO_2 nanosheet was restricted by the treatment of $TiCl_4$. However, the TiO_2 layer might not be enough to get rid of the back reaction on SnO_2 nanosheet film. The reason for the low photocurrent might

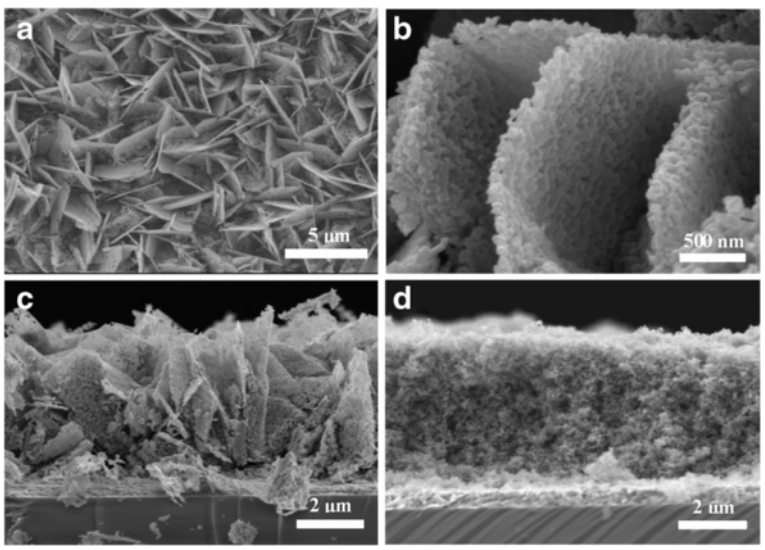

Fig. 3 SEM of the prepared films. **a**, **b** Top view of pure SnO_2 film. **c** Cross section of pure SnO_2 film. **d** Cross section of SnO_2/TiO_2 hybrid film

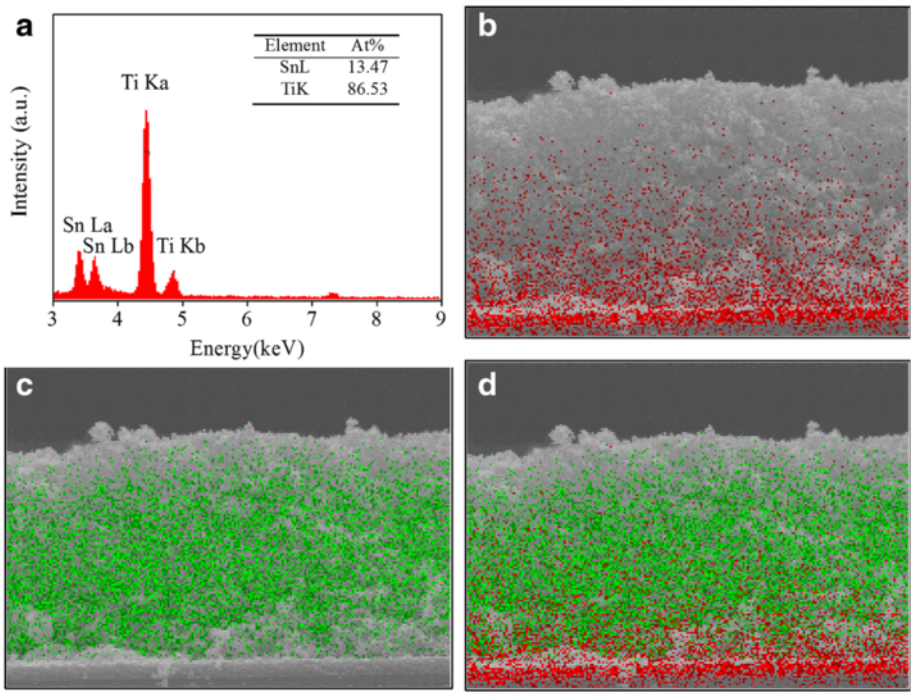

Fig. 4 EDS of the prepared films. **a** Sn and Ti content. **b** Sn element distribution map. **c** Ti element distribution map. **d** Combination of Sn and Ti element distribution map

be attributed to the low quantity of QDs on the photoelectrode. The specific surface area is a major factor affecting the loading of QDs. Those are also the reasons why the characteristic parameters are lower than that of the former reports [11–13]. To solve this problem, commercial TiO_2 nanoparticles (P25) were deposited on the SnO_2 nanosheet films. From Fig. 4, it can be seen that the photoelectric conversion properties of the photoanode are significantly improved. The J_{SC}, V_{OC}, and fill factor (*FF*) are about 13.0 mA cm^{-2}, 514 mV, and 52.2 %, respectively. The total photoelectric conversion efficiency (η) is about 3.49 %. There might be two reasons for the improvement of the photoelectric properties after the deposition of commercial TiO_2 nanoparticles (P25). One is the significant improvement of the specific surface area, the film electrode. The other reason is that the deposition of commercial TiO_2 nanoparticles (P25) further isolated SnO_2 from QDs and electrolyte, which further restricted the recombination of the photoexcited electron in the SnO_2 conductive band. As a reference, pure TiO_2 nanoparticles were also directly deposited on the FTO substrate under the same electrophoretic time as that used in the former experiments. The photoelectric conversion efficiency is about 2.51 % which is much lower than that of QDSCs assembled with SnO_2/TiO_2 hybrid films. All the characteristic parameters are shown in Table 1.

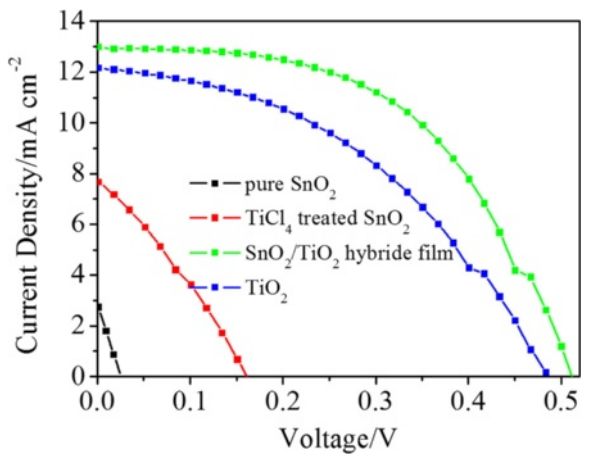

Fig. 5 *J-V* characteristic of the prepared CdS/CdSe co-sensitized QDSCs

Figure 6 shows the IPCE spectra of QDSCs assembled with these different photoanodes. IPCE spectra reflect the light response of photovoltaic devices at different

Table 1 Detailed photovoltaic parameters of the QDSCs obtained from Fig. 5

Photoanodes	V_{OC} (mV)	J_{SC} (mA cm^{-2})	FFP (%)	Efficiency (%)
SnO_2	25	2.9	23.8	0.02
$SnO_2 + TiCl_4$	161	7.7	29.7	0.37
$SnO_2 + TiCl_4$ + P25	514	13.0	52.2	3.49
P25	488	12.2	42.0	2.51

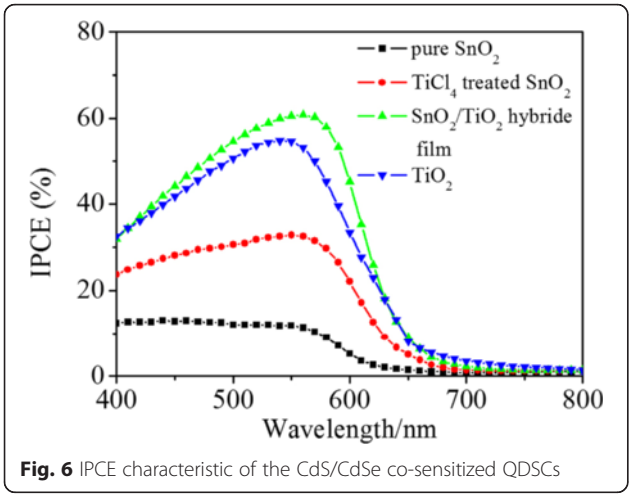

Fig. 6 IPCE characteristic of the CdS/CdSe co-sensitized QDSCs

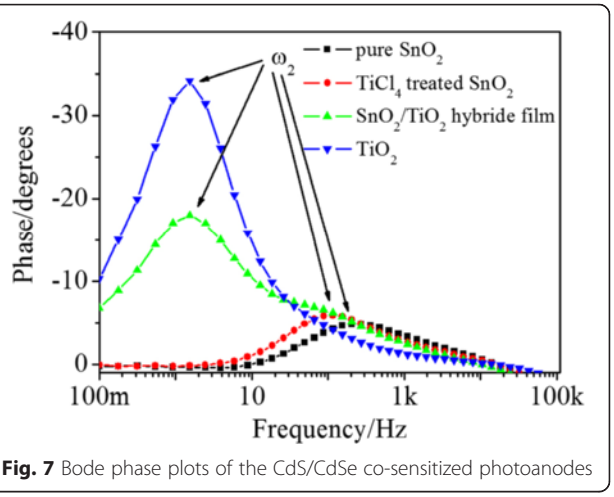

Fig. 7 Bode phase plots of the CdS/CdSe co-sensitized photoanodes

light wavelengths, which is directly related to photocurrent density and can be calculated from Eq. 4.

$$\mathrm{IPCE}\ (\%) = 1240 J_{\mathrm{SC}}/(\lambda P_{\mathrm{in}}), \tag{4}$$

where J_{SC} is the short circuit photocurrent density at a single wavelength, λ is the wavelength of the incident light, and P_{in} is the power of the incident light. The light absorbed by the photoanodes ranged from 400 nm to about 700 nm which is in accordance with the absorption range of CdS and CdSe. Comparing the curves obtained by different photoanodes, it can be seen that $TiCl_4$ treatment and TiO_2 nanoparticle coverage dramatically enhanced the IPCE values during the 400–700 nm, which is in accordance with the results of *J-V* curves.

Electrochemical impedance spectroscopy (EIS) is an efficient method to investigate the recombination process of the photoexcited electrons. EIS was carried out on SnO_2, $TiCl_4$-treated SnO_2, SnO_2/TiO_2 hybrid film, and TiO_2 film photo-electrodes under dark condition. A bias potential, −0.6 V, was applied in the testing process. Figure 7 shows the Bode phase plots of the QDSCs assembled with SnO_2, $TiCl_4$-treated SnO_2, SnO_2/TiO_2 hybrid film, and TiO_2 film. According to the previous work, there should be an electrochemical process (ω1) at high frequency (10^3–10^5 Hz) to correspond to the charge-transfer processes occurring at the counter electrode/electrolyte interface [21]. But it is not obvious in this experiment. However, there is an obvious electrochemical reaction process at the frequency range from about 1 to 10^3 Hz which was marked as ω_2. This process corresponds to the charge-transfer processes occurring at the SnO_2 ($TiCl_4$-treated SnO_2 film, SnO_2/TiO_2 hybrid film, or P25 film)/electrolyte (or QD) interface [21]. The characteristic frequency of ω_2 may reflect the electron lifetimes (τ_e) of the injected electrons [22]. The lifetimes (τ_e) of the photoexcited electron in the photoanodes were determined using the following equation (Eq. 5):

$$\tau_e = \frac{1}{2\pi f_{\max}}. \tag{5}$$

The characteristic frequency of these photoanodes, SnO_2, $TiCl_4$-treated SnO_2, SnO_2/TiO_2 hybrid film, and pure TiO_2 film, were 202.7, 115.4, 1.5, and 1.5 Hz, respectively. According to Eq. 5, the electron lifetimes (τ_e) were calculated to be about 0.8, 1.4, and 106.2 ms for the SnO_2, $TiCl_4$-treated SnO_2, SnO_2/TiO_2 hybrid film, and TiO_2 electrodes, respectively. It can be seen that $TiCl_4$ treatment exactly inhibited the recombination reaction of SnO_2 nanosheet electrode. But the effects of $TiCl_4$ treatment are very finite. After the coverage of TiO_2, the electron lifetime was lengthened by two orders to the same value as that of the pure TiO_2 photoanode. It can be seen that the SnO_2/TiO_2 hybrid electrode might combine the advantages of both SnO_2 nanosheet and TiO_2 nanoparticle. This result is in accordance with the *J-V* curves.

Conclusions

SnO_2 nanosheet-structured films were prepared using ZnO nanosheet as template. The as-prepared SnO_2 nanosheets contained plenty of nano-voids and were generally vertical to the substrate. TiO_2 nanoparticles were homogeneously deposited into the intervals between SnO_2 nanosheets to prepare hierarchically structured SnO_2/TiO_2 hybrid film. The hybrid films were co-sensitized with CdS and CdSe quantum dots. The photoinduced electron showed the same lifetimes in this SnO_2/TiO_2 hybrid film as that in the pure TiO_2 particles films. But the SnO_2/TiO_2 hybrid film photoanode had higher IPCE than pure TiO_2 nanoparticle photoanode. The total photoelectric conversion efficiency was about 3.49 %.

Competing Interests
The authors declare that they have no competing interests.

Authors' contributions
ZC and CCW carried out the experiment. WL, WPK, CLD, and ZLZ analyzed the data and finished the figures of the manuscript. SJL and WFZ modified the manuscript. All authors read and approved the final manuscript.

Acknowledgements
This work was supported by the Natural Science Foundation of China (No. 51304062, 21403056, and U1404202).

Received: 22 January 2016 Accepted: 23 May 2016
Published online: 14 June 2016

References

1. Hanna MC, Nozik AJ (2006) Solar conversion efficiency of photovoltaic and photoelectrolysis cells with carrier multiplication absorbers. J Appl Phys 100:074510
2. Mu LL, Liu CM, Jia JG, Zhou XW, Lin Y (2013) Dual post-treatment: a strategy towards high efficiency quantum dot sensitized solar cells. J Mater Chem A 1:8353
3. Hyun BR, Zhong YW, Bartnik AC, Sun LF, Abruna HD, Wise FW, Goodreau JD, Matthews JR, Leslie TM, Borrelli NF (2008) Electron injection from colloidal PbS quantum dots into titanium dioxide nanoparticles. ACS Nano 2:2206
4. Zhou R, Niu HH, Zhang QF, Uchaker E, Guo ZQ, Wan L, Miao SD, Xu JZ, Cao GZ (2015) Influence of deposition strategies on CdSe quantum dot-sensitized solar cells: a comparison between successive ionic layer adsorption and reaction and chemical bath deposition. J Mater Chem A 3:12539
5. Yan KY, Chen W, Yang SH (2013) Significantly enhanced open circuit voltage and fill factor of quantum dot sensitized solar cells by linker seeding chemical bath deposition. J Phys Chem C 117:92
6. Senevirathna MKI, Pitigala PK, Premalal EVA, Tennakone K, Kumara GRA, Konno A (2007) Stability of the SnO_2/MgO dye-sensitized photo electrochemical solar cell. Sol Energy Mater Sol Cells 91:544
7. Jarzebski ZM, Marton JP (1976) Physical properties of SnO_2 materials. 1. Preparation and defect structure. J Electrochem Soc 123:C199
8. Hendry E, Koeberg M, O'Regan B, Bonn M (2006) Local field effects on electron transport in nanostructured TiO_2 revealed by terahertz spectroscopy. Nano Lett 6:755
9. Tebby Z, Uddin T, Nicolas Y, Olivier C, Toupance T, Labrugère C, Hirsch L (2011) Low-temperature UV processing of nanoporous SnO_2 layers for dye-sensitized solar cells. ACS Appl Mater Interfaces 3:1485
10. Li SJ, Chen Z, Wang YY, Li T, Xu BH, Zhang WF (2014) Flexible photoanode for dye-sensitized solar cells with outstanding short-circuit current based on magnesium oxide-coated tin dioxide films. J Electrochem Soc 161:H1
11. Hossain MA, Yang GW, Parameswaran M, Jennings JR, Wang Q (2010) Mesoporous SnO_2 spheres synthesized by electrochemical anodization and their application in CdSe-sensitized solar cells. J Phys Chem C 114:21878
12. Hossain MA, Jennings JR, Koh ZY, Wang Q (2011) Carrier generation and collection in CdS/CdSe-sensitized SnO_2 solar cells exhibiting unprecedented photocurrent densities. ACS Nano 5:3172
13. Cánovas E, Moll P, Jensen SA, Gao YN, Houtepen AJ, Siebbeles LSA, Kinge S, Bonn M (2011) Size-dependent electron transfer from PbSe quantum dots to SnO_2 monitored by picosecond terahertz spectroscopy. Nano Lett 11:5234
14. Xiao JY, Huang QL, Xu J, Li CH, Chen GP, Luo YH, Li DM, Meng QB (2014) CdS/CdSe co-sensitized solar cells based on a new SnO_2 photoanode with a three-dimensionally interconnected ordered porous structure. J Phys Chem C 118:4007
15. Li Y, Guo YQ, Tan RQ, Cui P, Li Y, Song WJ (2013) Synthesis of SnO_2 nano-sheets by a template-free hydrothermal method. Mater Lett 63:2085
16. Fei L, Xu Y, Chen Z, Yuan B, Wu XF, Hill JS, Lin QL, Deng SG, Andersen P, Lu YF, Luo HM (2013) Preparation of porous SnO_2 helical nanotubes and SnO_2 sheets. Mater Chem Phys 140:249
17. Dong CJ, Liu X, Xiao XC, Chen G, Wang YD, Djerdj L (2014) Combustion synthesis of porous Pt-functionalized SnO_2 sheets for isopropanol gas detection with a significant enhancement in response. J Mater Chem A 2:20089
18. Desai UV, Xu CK, Wu JM, Gao D (2013) Hybrid TiO_2-SnO_2 nanotube arrays for dye-sensitized solar cells. J Phys Chem C 117:3232
19. Kalanur SS, Chae SY, Joo OS (2013) Transparent $Cu_{1.8}S$ and CuS thin films on FTO as efficient counter electrode for quantum dot solar cells. Electrochim Acta 103:91
20. Kay A, Grätzel M (2002) Dye-sensitized core-shell nanocrystals: improved efficiency of mesoporous tin oxide electrodes coated with a thin layer of an insulating oxide. Chem Mater 14:2930
21. Tian JJ, Zhang QF, Zhang LL, Gao R, Shen LF, Zhang SG, Qu XH, Cao GZ (2013) ZnO/TiO_2 nanocable structured photoelectrodes for CdS/CdSe quantum dot co-sensitized solar cells. Nanoscale 5:936
22. Kern R, Sastrawan R, Ferber J, Stangl R, Luther J (2002) Modeling and interpretation of electrical impedance spectra of dye solar cells operated under open-circuit conditions. Electrochim Acta 47:4213